

Article

Geomorphological Evolution of Volcanic Cliffs in Coastal Areas: The Case of Maronti Bay (Ischia Island)

Luigi Massaro , Giovanni Forte , Melania De Falco  and Antonio Santo 

Department of Civil, Architectural and Environmental Engineering, Università degli Studi di Napoli Federico II, 80125 Naples, Italy; giovanni.forte@unina.it (G.F.); melania.defalco@unina.it (M.D.F.); santo@unina.it (A.S.)

* Correspondence: luigi.massaro@unina.it

Abstract: The morphoevolution of coastal areas is due to the interactions of multiple continental and marine processes that define a highly dynamic environment. These processes can occur as rapid catastrophic events (e.g., landslides, storms, and coastal land use) or as slower continuous processes (i.e., wave, tidal, and current actions), creating a multi-hazard scenario. Maronti Bay (Ischia Island, Southern Italy) can be classified as a pocket beach that represents an important tourist and environmental area for the island, although it has been historically affected by slope instability, sea cliff recession, and coastal erosion. In this study, the historical morphoevolution of the shoreline was analysed by means of a dataset of aerial photographs and cartographic information available in the literature over a 25-year period. Furthermore, the role of cliff recession and its impact on the beach was also explored, as in recent years, the stability condition of the area was worsened by the occurrence of a remarkable landslide in 2019. The latter was reactivated following a cloudburst on the 26th of November 2022 that affected the whole Island and was analysed with the Dem of Difference technique. It provided an estimate of the mobilised volumes and showed how the erosion and deposition areas were distributed and modified by wave action. The insights from this research can be valuable in developing mitigation strategies and protective measures to safeguard the surrounding environment and ensure the safety of residents and tourists in this multi-hazard environment.



Citation: Massaro, L.; Forte, G.; De Falco, M.; Santo, A. Geomorphological Evolution of Volcanic Cliffs in Coastal Areas: The Case of Maronti Bay (Ischia Island). *Geosciences* **2023**, *13*, 313. <https://doi.org/10.3390/geosciences13100313>

Academic Editors: Jesus Martinez-Frias, Saverio Romeo, Francesco Mugnai, Mauro Bonasera, Roberta Boni and Ciro Cerrone

Received: 29 September 2023
Revised: 13 October 2023
Accepted: 16 October 2023
Published: 17 October 2023



Copyright: © 2023 by the authors. Licensee MDPI, Basel, Switzerland. This article is an open access article distributed under the terms and conditions of the Creative Commons Attribution (CC BY) license (<https://creativecommons.org/licenses/by/4.0/>).

Keywords: coastal areas; beach dynamics; cliff retreat; landslide; erosion rates

1. Introduction

Coastal areas undergo frequent landscape changes due to the interactions of multiple continental and marine processes that generate a highly dynamic environment. Landscape changes can occur as a consequence of rapid catastrophic events and/or slower continuous processes operating in a wide range of scales. These processes include landslides, storms, and coastal land use, as well as wave, tidal, and current actions.

Shoreline erosion is one of the main hazards affecting coastal areas. These processes include tsunamis, river flooding, and landslides. In some cases, these processes are strictly connected, like in the case of soil erosion, where beach retreat and cliff instability lead to landslides, generating a complex multi-hazards scenario. In turn, the cliff erosion rates are connected to the geological features of the area, including the mechanical strength of the rock masses and the geometric properties of the fracture system [1–3].

Assessment of the erosion processes and quantification of coastal retreat are critical for proper coastal planning and engineering mitigation [4–6]. In some areas, a coastal hazard is determined by a high rate of coastal retreat, which causes important loss of land and, therefore, money, infrastructure, and human life. Moreover, in recent years, coastal erosion has generally worsened due to the increasing occurrence of extreme meteorological events (e.g., typhoons, hurricanes, and coastal storms), stronger winds and waves, and sea level rise, all connected to global climate change [7–11]. Additionally, sediment fluxes from continental and rock coast erosion represent about 2% ($\sim 0.4 \text{ Gt a}^{-1}$) of the global flux, and it has an impact on the chemistry of the ocean [12,13].

Several methods are applied to assess the overall coastal hazard, including monitoring and evaluating geological features [14–17] and individual hazards [18] characterising the area. Nevertheless, the understanding of coastal erosion phenomena is difficult due to the occurrence of multiple triggering factors that interact on different spatial and temporal scales [19–21].

This study focused on the coastal evolution of Maronti Bay (on the southern part of Ischia Island) in the municipalities of Barano and Serrara Fontana. Ischia Island has been intensely affected by slope stability phenomena connected to volcanic activity, earthquakes, stormy rains, and/or coastal erosion [22–28]. In particular, this area was historically characterised by coastal erosion processes as well as slope instabilities and is currently affected by a wide retrogressive debris avalanche threatening the uphill urban centre (Figure 1).



Figure 1. Aerial photograph of the 26th November 2022 landslide with the affected buildings on the cliff top.

The historical morphoevolution of the coastal area of Maronti was analysed by means of a dataset of aerial photographs and cartographic information available in the literature. The collection and interpretation of these resources enabled the reconstruction of a chronological sequence of the erosion/progradation phases of the shoreline over the years and the understanding of the role of cliff recession and its impact on beach use.

Furthermore, a focus on the landslide event that occurred on 26th November 2022 was carried out through drone surveys to evaluate the difference between the pre- and

post-landslide DEMs. This analysis enabled the estimation of the mobilised volumes and the investigation of the reactivation and evolution of the landslide.

The adopted approach, combining historical data, aerial photography, cartography, and Virtual Outcrop Model (VOM) remote analysis, provided a geometrical understanding of the coastal cliff evolution and the impact of landslides in the study area. These findings are essential for better understanding and the management of landslide risks on Ischia. The insights from this research can be valuable in developing mitigation strategies and protective measures to safeguard the surrounding environment and ensure the safety of residents and visitors in this region.

2. Study Area

2.1. Geological Setting

Ischia Island is part of the Phlegraean Fields volcanic complex, and it extends for about 42 km² into the Gulf of Naples (Figure 2). The geological and geomorphological characteristics of the island make it highly susceptible to various instability events, including earthquakes, flow-like landslides, rockfalls, flash floods, and tsunamis, resulting in a multi-hazard environment [24,29]. The prevalent lithologies on the island are trachytes and latite-phonolites lavas, accompanied by pyroclastic soils and ancient mudflow deposits [30,31].

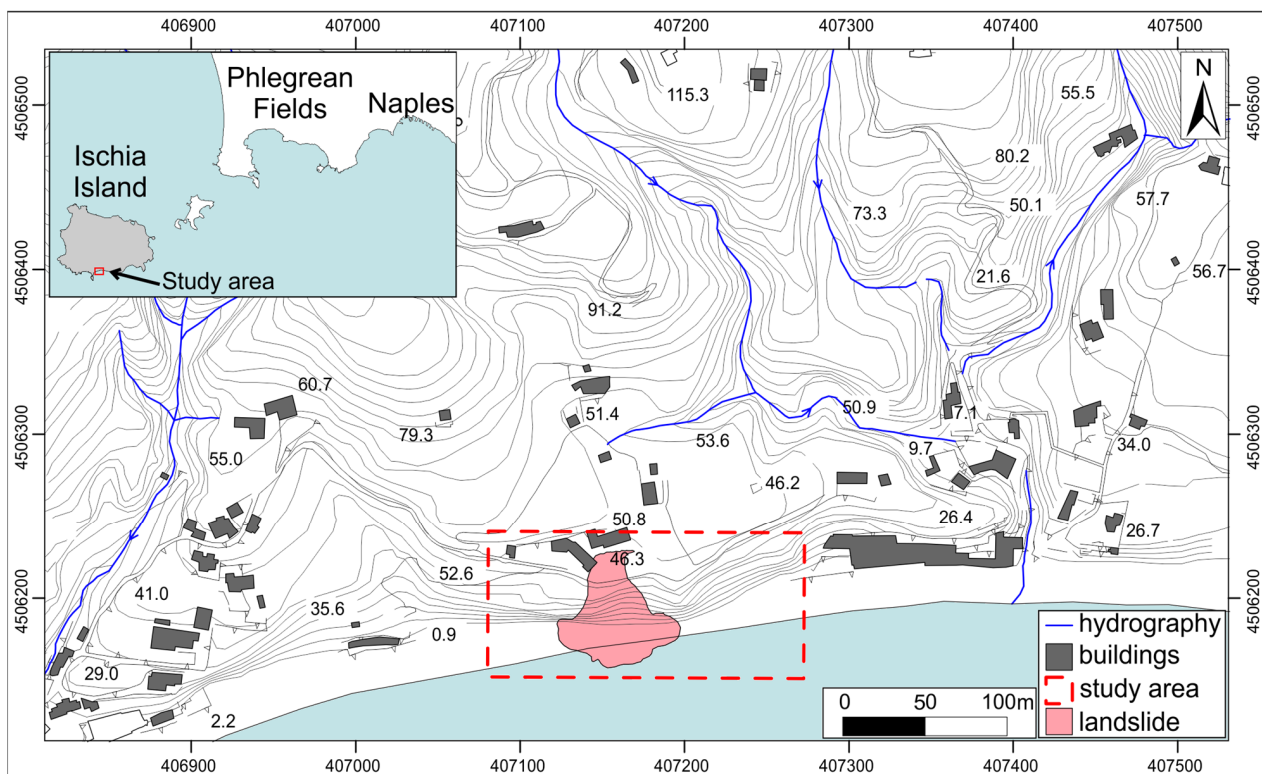


Figure 2. Topographic map (2015) of Maronti Bay with the location of the study area and the 2020 landslide body.

The first volcanic activity on Ischia Island dates back over 150 ka, with the most recent significant eruption being the Arso eruption in 1302 [30–32]. The overall volcanic activity is generally divided into five major phases that are further grouped into two main cycles, separated by a quiescent period of around 25 ka and distinguished by the emplacement of the Green Tuff formation (~55 ka). The Green Tuff forms the core of Mt. Epomeo and is a trachytic ignimbrite, exhibiting a green colour due to alteration from contact with seawater.

Maronti Bay is situated in the municipalities of Barano and Serrara Fontana, and it represents an important coastal sector of the island with high environmental and tourist

value. Overall, the southern part of Ischia is mainly composed of high coasts forming a series of bays, with Maronti Bay in the central zone. The height of the Maronti cliffs increases from east to west, in a 50 to 120 m a.s.l. range. Along the coast, three main debris flow units can be identified, exhibiting different lithological and textural characteristics [33]:

- In the eastern sector there is a gravel-size (1–10 cm) grain-supported debris flow unit, with a sandy matrix and a light beige colour. The clasts comprise siltites of Colle Jetto, Tufite, tuffs, and lavas, appearing with both sharp and rounded edges;
- Below the latter unit, there is another debris flow body, with an olive-green colour, exposed in the central sector of the coastal area. Its thickness varies from 2 to about 10 m. This unit is mainly composed of clasts of Colle Jetto siltites and small inclusions of Tufite and lava;
- In turn, the latter unit has an erosive contact with another debris flow body in the central–western sector of Maronti beach. This unit is mainly composed of clasts of dark green Tufite, occasionally containing sub-rounded inclusions of siltites of Colle Jetto and lavas.

2.2. Historical Cliff Instability

The Maronti cliff undergoes significant erosive action from the sea as it lacks adequate protection from a sufficiently wide beach. The wave action plays a critical role in the cliff retreat process by exerting stress at the cliff base and by infiltrating within the fracture system and pore space of the rock mass [34–36]. The wave motion creates beach notches of various depths, particularly evident in tuffaceous deposits where some of them can reach several meters in depth, which highlights the influence of the mechanical properties of the lithology in the erosion process [1,3].

The beach underwent intense regression from 1970 to 1999, and in May 2002 an artificial nourishment project brought the beach to widths of 40–80 m in the western sector, 20–30 m in the central sector, and about 10 m in the eastern sector [37].

The coastal area of Maronti has been affected by several landslide events [25], especially in the western–central sector, documented by historical pictures during the last century. Since 1970, a total of 14 landslide events have been distinctly reported and documented, as summarised in Table 1.

Table 1. Landslide events that affected the coastal area of Maronti from 1970 (modified after Del Prete and Mele [25] and references therein).

Location	Date	Landslide Type	Deposit type	Sources	Damages
Testaccio-Maronti	March 1970	Rotational sliding	Tuffs, pyroclastic deposits, and detrital deposits	Il Mattino, 1970; Il Mattino, 1978	Destruction of “Testaccio-Maronti” road at km 1 + 800
Lido dei Maronti	7 June 1978	Rockfall evolving into a debris flow	Detrital deposits	Il Mattino, 1978	Invasion of the beach area and 5 fatalities
Lido dei Maronti (Fumarole)	2 August 1983, 4 August 1983	Rockfall	Detrital deposits	Il Mattino, 1983	Invasion of the beach area and destruction of “Alba Marina” beach establishment with 1 injured person
Lido dei Maronti	22 February 1987	Rockfall	Detrital deposits	Pellegrino, 1994	Damage to Hotel Vittoria
Lido dei Maronti	14 October 1989	Rockfall	Detrital deposits	Pellegrino, 1994	Information not available
Lido dei Maronti	6 November 1990	Rockfall	Detrital deposits	Il Mattino, 1990	No damages reported
Lido dei Maronti	September 1997	Rockfall	Detrital deposits	Field surveys	Invasion of the beach area and damages in Via Maronti and to private buildings
Lido dei Maronti	28 December 1998	Rockfall	Detrital deposits	Field surveys	No damages reported

Table 1. *Cont.*

Location	Date	Landslide Type	Deposit type	Sources	Damages
Lido dei Maronti	30 September 1999	Rockfall	Detrital deposits	Enti, Il Golfo, 1999	Invasion of the beach area and damages in Via Maronti and to private buildings
Lido dei Maronti	27–28 December 1999	Rockfall	Detrital deposits	Il Golfo, 1999 e 2000	No damages reported
Lido dei Maronti	31 December 2000	Rockfall	Detrital deposits	Il Golfo, 2001	Invasion of the beach area
Lido dei Maronti	3 January 2001	Rockfall	Detrital deposits	Il Golfo, 2001	Invasion of the beach area
Lido dei Maronti	15 December 2020	Rockfall	Detrital deposits	La Repubblica, 2020	Invasion of the beach area and damages in Via Iesca
Lido dei Maronti	26 November 2022	Rockfall	Detrital deposits	Local team, 2022	Invasion of the beach area and damage to private buildings

This issue is due to the geological and geomorphological setting of Maronti Bay, as the presence of volcanic lithologies, steep cliffs, and erosion processes contribute to frequent landslide events [37]. The Maronti coastline, known for its environmental significance, experiences considerable erosion due to the impact of wave motion.

3. Data and Methods

The data collection was carried out by gathering historical photos, Google Earth images, maps, and LiDAR of the area from 1998 to 2023 (Table 2). The original dataset included additional historical pictures and maps. They were discarded due to distortions of the images and georeferencing issues. For this aim, the existing buildings above the cliff were used as checkpoints to validate the quality of the data. In addition, field surveys enabled the characterisation of the morphometric properties of 26 November 2022 landslide and image acquisition via drone for the construction of orthophotos, DEM, and Virtual Outcrop Models (VOM) of the cliff.

Table 2. List of satellite images, maps, and LiDAR collected to analyse the evolution of the Maronti beach area. Coordinate system: WGS84-UTM; zone: 33 North.

Data Type	Year	Source
Topographic Map (1:5000)	1998	Regione Campania
Topographic Map (1:5000) and Orthophoto	2004	
LiDAR (1 × 1 m)	2009	Città metropolitana
Satellite image	2013	Google Earth
	2014	
Topographic Map (1:5000) and Orthophoto	2015	Regione Campania
Satellite image	2016	Google Earth
	2019	
	2021	
LiDAR (1 × 1 m) and Orthophoto	2022	Protezione Civile
Orthophoto and DTM (1 × 1 m)	2023	Drone survey

The drone used for high-resolution image acquisition was a DJI™ Phantom 4 RTK quadrotor UAV platform equipped with a 4 K video camera with a 1/2.3" CMOS sensor, 94-degree field of view, 12.4 MP images, and a focal length of 3.6 mm. The flights were performed at a height of 100 m, defining a resolution (Ground Sample Distance) of 3 cm. The images were acquired with an overlap of 80% and a side lap of 70% and were succes-

sively processed with Structure from Motion (SfM) computer vision techniques (AgiSoft Metashape 2.0.3 software). The developed dense point cloud enabled the production of the Digital Surface Model (DSM), Digital Terrain Model (DTM), and the nadir and oblique orthomosaic images.

The satellite images were georeferenced by means of GIS software based on the Topographic Map (1:5000), using fixed reference points (e.g., buildings and crossroads). Successively, the cliff perimeter and the beach limits were digitised for each year on the available orthophotos, satellite images, and topographic maps, enabling the analysis of their temporal evolution and the assessment of coastal retreat (i.e., sea cliff-orthogonal translation from its initial position). The shoreline position was identified as the water line at the time of the individual images since the study area is located in a microtidal environment [38,39]. The progradation/regression trends of the cliff and beach edges were quantified by measuring their variation in sequential images. These values were collected along 10 measurement lines (transect, T) perpendicularly arranged with respect to the cliff and the beach (Figure 3).



Figure 3. Measurement lines (T1–T10) disposed along the cliff and the beach edges for the measurement of their progradation/regression evolution. Example of the 2022 orthophoto.

The DEMs from different years were quantitatively compared with each other by computing the DEM of Difference (DoD). In detail, the 2009–2022 and the 2022–2023 DoD were produced by using the 2009 and 2022 LiDAR-derived DTMs and the 2023 UAV-derived DTM. This method is commonly applied for volumetric Geomorphic Change Detection analyses [40–42] to highlight the main areas of erosion (cold colours) and accumulation (warm colours), as well as to compute an estimation of the mobilised volumes.

4. Results

4.1. Temporal Evolution

The collected dataset of maps and aerial photos enabled the measurement of the cliff and beach widths in different years. Successively, individual time ranges were defined depending on the data availability, allowing us to quantify the variation of the cliff retreat and beach extension through the years. For some years, the measurement of the cliff boundaries was not possible due to the low quality of the images; therefore, fewer time intervals were defined with respect to the beach analysis. For this reason, to ensure proper comparisons, the time ranges were compared in terms of annual rate. Furthermore, as the cliff perimeter can only show retrogression or no change, the values are shown as positive for simplicity. In Table 3, the values of the cliff retreat are summarised for the 10 measurement lines (T1–T10) and the 5 time ranges.

Table 3. Cliff variation for time ranges measured on the 10 measurement lines (T1–T10).

Time Range	T1	T2	T3	T4	T5	T6	T7	T8	T9	T10
	m	m	m	m	m	m	m	m	m	m
1998–2004	0.6	1.5	1.6	5.1	5.4	5.6	1.7	5.0	0.9	1.9
2004–2009	0.4	0.1	1.3	1.2	3.8	3.5	0.6	3.2	1.0	3.0
2009–2015	0.8	0.5	0.1	0.2	0.7	1.0	0.5	0.6	0.3	0.1
2015–2022	2.4	1.7	0.3	0.2	0.7	19.0	0.3	0.2	0.3	0.4
2022–2023	0.4	0.5	0.3	0.4	0.2	0.1	0.2	0.2	0.6	0.2

The cliff retreat rate was calculated and compared between time intervals for each transect (Figure 4). Since the 2023 drone survey was performed in June, the annual rate was calculated by considering that the cliff retreat measurements are not referring to an entire year. From this comparison, the following observations can be derived:

- The amount of cliff retreat is higher for the transects T4–T6, which represent the central part of the cliff (Figure 3) where the landslide events mainly occurred.
- The highest regression rate is registered in the 2015–2022 period on the T6 (about 271 cm year⁻¹), with the landslide event of the 26 November 2022 playing a primary role.
- On average, the 2022–2023 and the 2009–2015 intervals show the highest (about 61 cm year⁻¹) and the lowest (about 8 cm year⁻¹) cliff retreat rates, respectively.

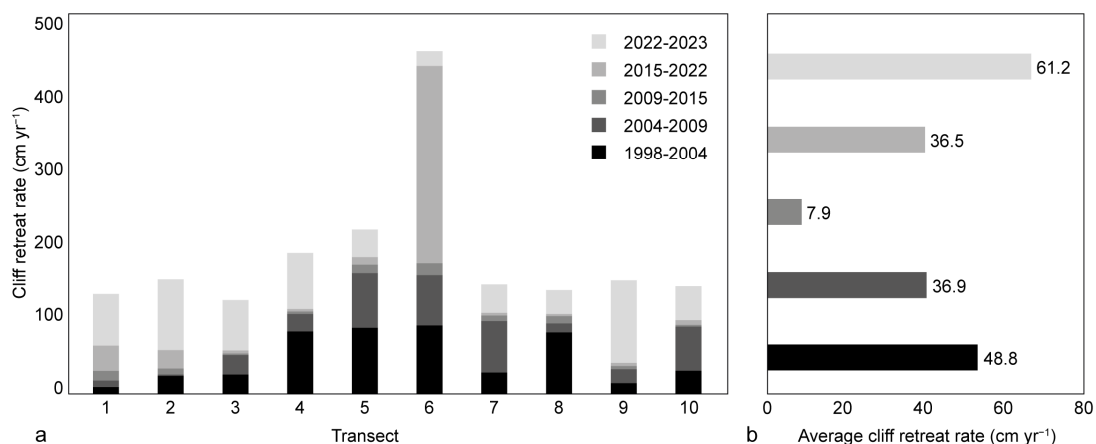


Figure 4. Cliff retreat rate (cm year⁻¹) measured on the 10 measurement lines at different time intervals. (a) Cumulative cliff retreat rate for each transect through the time; (b) average cliff retreat rate for each time interval.

In Table 4, the values of the beach width variation are summarised for the 10 measurement lines (T1–T10) during 10 time intervals.

Table 4. Beach width variation (m) for time ranges measured on the 10 measurement lines (T1–T10). The positive values indicate an increase in width, and the negative values indicate a decrease in width.

Time Range	T1	T2	T3	T4	T5	T6	T7	T8	T9	T10
	m	m	m	m	m	m	m	m	m	m
1998–2004	23.2	23.2	20.8	19.7	19.4	10.7	9.3	10.4	14.2	17.4
2004–2009	−29.6	−28.9	−25.4	−22.4	−17.4	−15.3	−16.7	−15.26	−16.9	−23.8
2009–2013	12.8	11.4	7.5	7.8	7.0	6.5	1.1	−1.1	−3.0	4.1
2013–2014	−2.8	−2.8	0.6	−3.1	−1.1	0.2	−0.1	0.0	−2.3	−9.7
2014–2015	12.2	13.0	8.9	9.0	5.1	2.7	7.9	12.4	15.7	17.3
2015–2016	−18.1	−21.0	−19.2	−15.8	−13.1	−10.5	−9.0	−12.4	−18.7	−20.0
2016–2019	3.4	7.3	5.6	4.7	4.3	3.6	1.3	5.0	6.7	12.1
2019–2021	−2.9	−5.3	−1.7	−1.5	−0.6	1.4	−1.3	−5.0	−6.7	−13.6
2021–2022	−5.0	−3.9	−4.0	−2.5	3.1	8.2	3.9	2.8	0.0	−3.6
2022–2023	−2.8	−1.7	−1.9	−3.7	−1.0	−0.1	1.7	3.0	5.4	5.9

Again, to ensure a proper comparison between the measurements, the rate of beach width variation was calculated (Figure 5). It can be noticed that the negative variation rates (beach decrease in width) symmetrically increase towards the external areas of the beach, with the T1–T2 and T10 displaying the highest values. This trend, as expected, is the opposite of what was observed for the cliff retreat (Figure 4). The trends of beach regression (negative values) and progradation (positive values) show a regular oscillation through time. In particular, the 2014–2015 and 2015–2016 time intervals show very high values of progradation (about 10 m yr^{−1}) and regression (about 16 m yr^{−1}), respectively. On the contrary, the average beach regression rate of the interval 2021–2022 was mitigated by the occurrence of the 26th November landslide, which created a remarkable cliff retreat (Figure 4) in T5–T8.

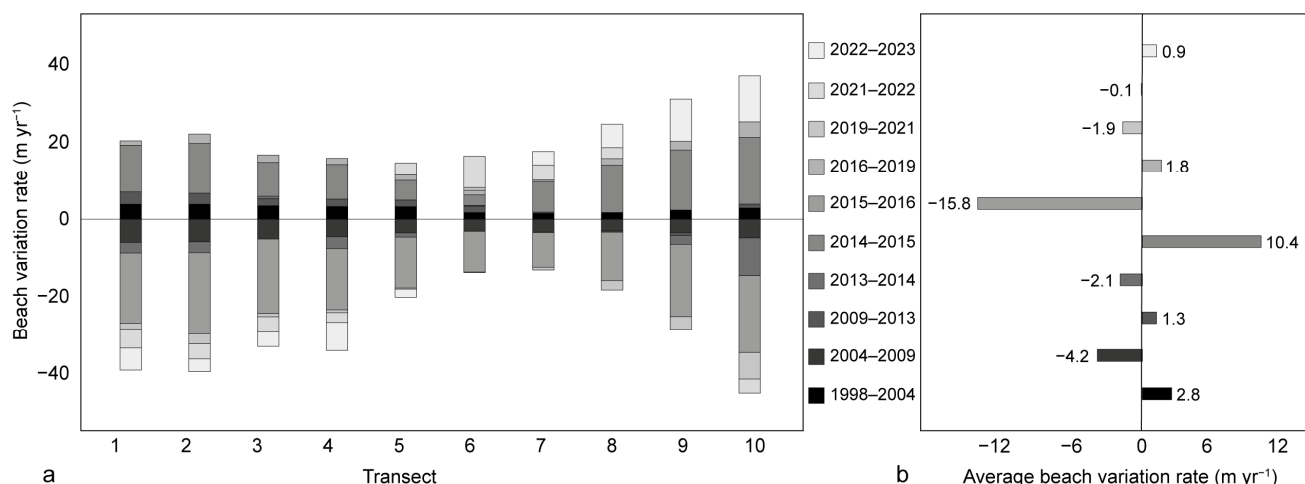


Figure 5. Beach width variation rate (m yr^{−1}) measured on the 10 measurement lines at different time intervals. (a) Cumulative beach width variation rate for each transect through the time; (b) average beach width variation rate for each time interval. The positive values indicate progradation, and the negative values indicate regression.

4.2. November 2022 Landslide

The landslide event of 26th November 2022 can be classified as a debris avalanche [43]. This phenomenon created a remarkable cliff retreat (about 19 m, Table 3) and a consequent enlargement of the beach area. This was due to the formation of a crown area in an inner

portion of the cliff and by the consequent invasion of the beach due to the deposition area, where debris and large blocks (up to 5–6 m³ of volume) can be found.

This landslide event was characterised by two drone surveys, obtaining orthophotos and 3D models, which were used to analyse the evolution of the landslide body. The area of the debris avalanche was measured from the two orthophotos (Figure 6), with values of 2828 m² in 2022 and 2177 m² in 2023 (Table 5).

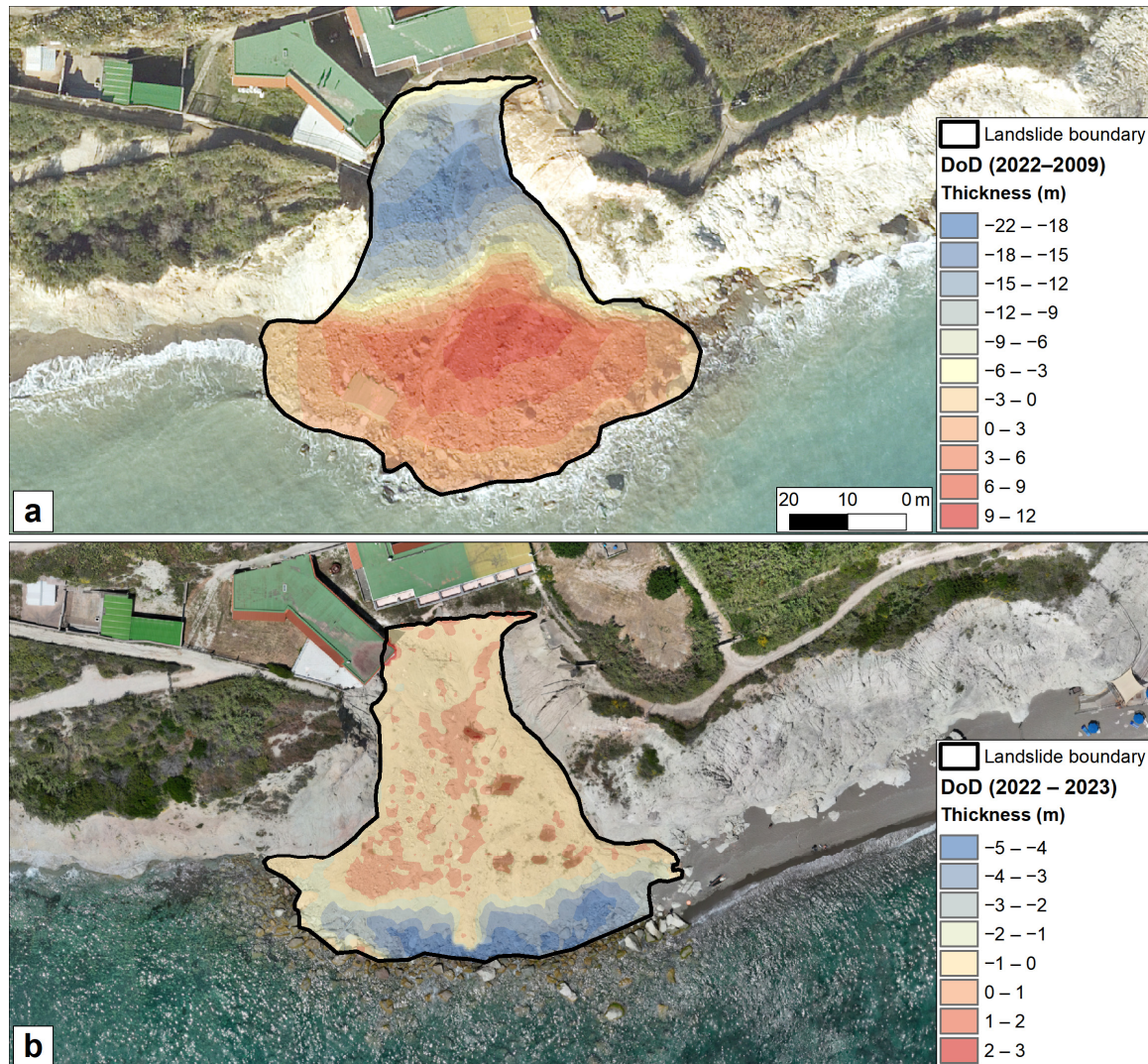


Figure 6. Orthophotos of the November 2022 landslide area with the landslide perimeter and the results of the DoD analyses between (a) 2009–2022 and (b) 2022–2023 DEMs.

Table 5. Quantified areal and volume data of the 26th November 2022 landslide.

Time Interval	Landslide Area	Average Erosion Thickness	Average Deposition Thickness	Eroded Volume	Deposited Volume
	m ²	m	m	m ³	m ³
2009–2022	2828	−10.5	4.6	29,700	13,000
2022–2023	2176	−1.2	0.3	2600	650

The DEMs produced from field surveys in 2022 and 2023 were compared with each other and with the 2009 DEM, which represents a pre-landslide baseline. The resulting

DoDs were analysed to estimate the mobilised volumes and to identify the areas of erosion and accumulation. The comparison with the pre-landslide model (2009) defines a clear separation between the crown and the deposition areas (Figure 6a). In this case, an eroded volume of 29,700 m³ and a deposited volume of 13,000 m³ were estimated from the DoD (Table 5), assuming average values of thickness of 10.5 m eroded and 4.6 m deposited.

Successively, the 2022–2023 DoD was computed, and a different scenario was observed. In this time range, the original crown area underwent minor movement of material, while the landslide toe showed high erosion (Figure 6b), mainly due to the action of the waves. In this case, the estimation of the eroded volume was 2600 m³, and the deposited volume was 650 m³ (Table 5), with an average eroded thickness of 1.2 m and an average deposited thickness of 0.3 m.

5. Discussion

In this study, the morphoevolution of the coastal area of Maronti Bay (Ischia Island) was investigated over a period of 25 years. This analysis enabled the quantification of the cliff retreat rates and the variation of the beach width. The cliff showed constant regression through the years, with higher rates in the central sector of the analysed cliff (T4–T6, Figure 4). In general, the cliff retreat rate underwent remarkable acceleration in recent years (2022–2023), with average cliff retreat rates of 36.5 cm year⁻¹ in 2015–2022 and 61.2 cm year⁻¹ in 2022–2023. Also, it should be considered that the 2015–2022 time interval underestimates the November 2022 landslide contribution, since the total cliff retreat registered is divided for the time range. The observed cliff retreat increase is mainly due to the landslide activity that started in 2019, had a main event on 26 November 2022, and is still active.

The evolution of the beach width showed an alternation of regression and progradation trends. In detail, the regression trends (the negative parts of the chart in Figure 5) can be correlated with the cliff retreat trends (Figure 4). In fact, the areas where the highest cliff retreat rates were registered (T4–T6) showed lower beach regression rates with respect to the other transects. The trends of beach regression and progradation showed low or no correlation with the cliff retreat rate, with the increase/decrease of beach width alternating independently of the cliff.

The total balance of the 25-year comparison (Figure 7) showed that the cliff retreated from a minimum of 3.0 m (T9) to a maximum of 29.1 m (T6), while the beach increased in width in the central part of the analysed area (T6, 10.0 m) and displayed a maximum decrease of 4.4 m (T9). This shoreline evolution can be considered as part of the same process observed by Giordano, Ferrante, Marsella and Vicinanza [37], who found that the area of Maronti is characterised by strong seaward sediment transport.

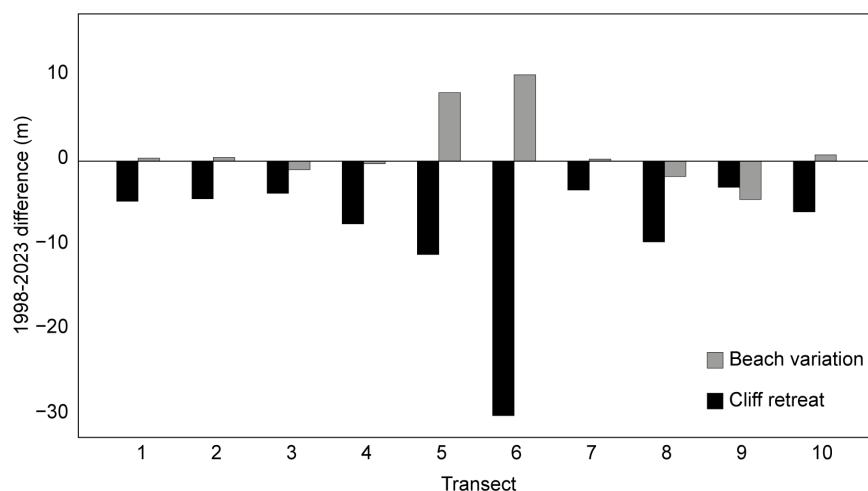


Figure 7. Absolute cliff and beach width variations from 1998 to 2023.

The effects of coastal erosion should be considered as primary elements increasing the risk of coastal landslides. Young et al. [44] showed that areas characterised by frequent wave impacts undergo higher (up to five times) sea cliff erosion rates, although rain usually represents the main trigger. Therefore, the prediction of landslides in such environments is strictly connected to the assessment of the magnitude and rate of coastal erosion [45].

The landslide event of 26 November 2022 represented a main event within a complex deformation process that started in 2019 and is still ongoing. The 2009–2022 DoD analysis provided a pre-landslide comparison, allowing us to estimate the total mobilised volume at about 29,700 m³. On the other hand, the 2022–2023 DoD highlighted the current reactivation of the landslide, with deposition of new material in the proximal part and erosion by the wave action in the distal part (toe).

In both cases, the total mobilised volume is not as directly distributed as the deposited one (Table 5), defining a difference in volume (56% and 75% of the total eroded volumes in 2009–2022 and 2022–2023, respectively). These different results can be explained by the actions of the different processes. In the first time interval, the erosion volume was mainly due to the landslide events and, in a minor part, to the wave action. Conversely, in the second time interval, the eroded volume was determined mainly by the wave action. The role played by the wave action was confirmed by the wind data collected from the Naples monitoring station (ISPRA) for the 2010–2023 interval (Figure 8). These data showed that the winds from the SW represented the most intense (up to 13.9 m s⁻¹) winds affecting the coastal area of Maronti. Also, the sea storm recorded in the 1998–2023 time interval on Maronti beach showed that the wave motion from the SW represented the most intense (>3 m wave height) and frequent trend [37].

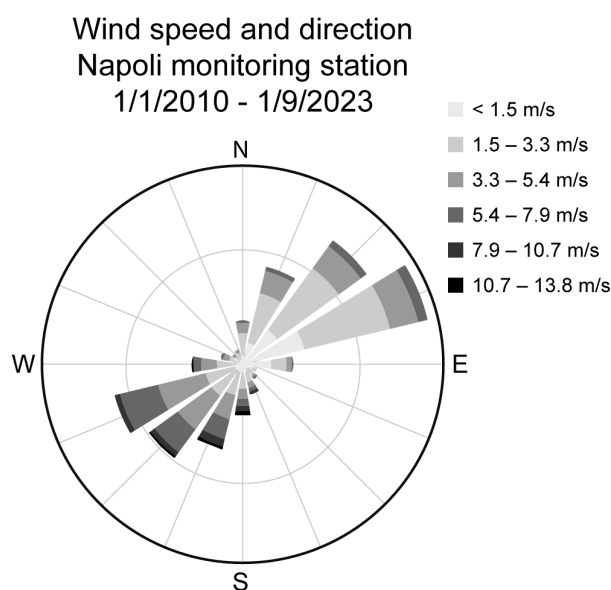


Figure 8. Wind direction and intensity recorded at Napoli monitoring station in the 2010–2023 time interval (ISPRA).

In this study, a limitation of the approach adopted for the coastal erosion analysis is the simplification of the coastal evolution processes, which are much more complex due to interactions among sea cliff collapse, weathering, wave action, and sea level fluctuation [46]. However, such an approach for the assessment of erosion and retreat rates allowed us to investigate the interactions of coastal processes and landslide activity.

The case study of Maronti Bay is a clear example of coastal erosion affecting the sea cliff collapses with a retrogressive trend. In fact, the areas where the beach displayed an increase in width in the 25-year analysis are strictly related to the debris production due to the landslide and the consequent cliff retreat. Such evolution of the sea cliff represents a

major hazard to the area above the cliff, which is intensely populated and hosts important road network branches.

6. Conclusions

In conclusion, a combination of historical data, aerial photographs, cartography, and VOM remote analysis provided a comprehensive understanding of the coastal cliff evolution and the impact of landslides in the study area that can be summarised as follows:

- This is a relevant case study for multi-hazards, as characterized by a high slope instability as well as accelerated coastal erosion;
- In 25 years of historical analysis, the coastline mainly regressed despite the high production of debris coming from the failures of the sea cliff;
- These two processes were strongly related, as the main morphogenetic agent of the area was represented by the impact of the waves;
- The recent debris avalanche was studied in detail through the DoD approach, enabling an estimation of the total mobilised volume of about 29,700 m³.

These findings are essential for a better understanding of the complex morphoevolution of Maronti Bay and the management of ground instabilities on the whole island. In fact, this type of coastal hazard impacts a built environment as well as economic activities. The insights from this research can be valuable in developing mitigation strategies and protective measures to ensure the safety of residents and tourists in this multi-hazard environment.

Author Contributions: Conceptualization, G.F.; methodology, G.F. and L.M.; software, L.M. and M.D.F.; validation, L.M., G.F. and M.D.F.; investigation, G.F., M.D.F. and A.S.; data curation, L.M.; writing—original draft preparation, L.M.; writing—review and editing, L.M., G.F. and M.D.F.; visualization, L.M. and M.D.F.; supervision, G.F.; project administration, A.S.; funding acquisition, A.S. All authors have read and agreed to the published version of the manuscript.

Funding: The work included in this study benefited from the support of DPC ReLUIIS project funded by the University of Naples (P.I. Antonio Santo).

Data Availability Statement: The data will be provided upon request.

Acknowledgments: Ermanno Marino is acknowledged for the drone surveys. The Authors are grateful to the Editor and three anonymous reviewers for their fruitful insights and comments.

Conflicts of Interest: The authors declare no conflict of interest.

References

1. Benumof, B.T.; Storlazzi, C.D.; Seymour, R.J.; Griggs, G.B. The relationship between incident wave energy and seacliff erosion rates: San Diego County, California. *J. Coast. Res.* **2000**, *16*, 1162–1178.
2. Bonasera, M.; Cerrone, C.; Caso, F.; Lanza, S.; Fubelli, G.; Randazzo, G. Geomorphological and Structural Assessment of the Coastal Area of Capo Faro Promontory, NE Salina (Aeolian Islands, Italy). *Land* **2022**, *11*, 1106. [[CrossRef](#)]
3. Budetta, P.; Galietta, G.; Santo, A. A methodology for the study of the relation between coastal cliff erosion and the mechanical strength of soils and rock masses. *Eng. Geol.* **2000**, *56*, 243–256. [[CrossRef](#)]
4. Callaghan, D.P.; Roshanka, R.; Andrew, S. Quantifying the storm erosion hazard for coastal planning. *Coast. Eng.* **2009**, *56*, 90–93. [[CrossRef](#)]
5. Laksono, F.A.; Borzi, L.; Distefano, S.; Di Stefano, A.; Kovács, J. Shoreline Prediction Modelling as a Base Tool for Coastal Management: The Catania Plain Case Study (Italy). *J. Mar. Sci. Eng.* **2022**, *10*, 1988. [[CrossRef](#)]
6. Molina, R.; Anfuso, G.; Manno, G.; Gracia Prieto, F.J. The Mediterranean Coast of Andalusia (Spain): Medium-Term Evolution and Impacts of Coastal Structures. *Sustainability* **2019**, *11*, 3539. [[CrossRef](#)]
7. Elsner, J.B.; Kossin, J.P.; Jagger, T.H. The increasing intensity of the strongest tropical cyclones. *Nature* **2008**, *455*, 92–95. [[CrossRef](#)]
8. Wahl, T.; Plant, N.G. Changes in erosion and flooding risk due to long-term and cyclic oceanographic trends. *Geophys. Res. Lett.* **2015**, *42*, 2943–2950. [[CrossRef](#)]
9. Bengtsson, L.; Hodges, K.I.; Esch, M.; Keenlyside, N.; Kornbluh, L.; Luo, J.-J.; Yamagata, T. How may tropical cyclones change in a warmer climate? *Tellus A Dyn. Meteorol. Oceanogr.* **2007**, *59*, 539–561. [[CrossRef](#)]
10. Zhang, H.; Sheng, J. Examination of extreme sea levels due to storm surges and tides over the northwest Pacific Ocean. *Cont. Shelf Res.* **2015**, *93*, 81–97. [[CrossRef](#)]
11. Harley, M. Coastal Storm Definition. In *Coastal Storms*; Wiley Online Library: Hoboken, NJ, USA, 2017; pp. 1–21.

12. Syvitski, J.P.M.; Peckham, S.D.; Hilberman, R.; Mulder, T. Predicting the terrestrial flux of sediment to the global ocean: A planetary perspective. *Sediment. Geol.* **2003**, *162*, 5–24. [[CrossRef](#)]
13. Regard, V.; Prémaillon, M.; Dewez, T.J.B.; Carretier, S.; Jeandel, C.; Godderis, Y.; Bonnet, S.; Schott, J.; Pedoja, K.; Martinod, J.; et al. Rock coast erosion: An overlooked source of sediments to the ocean. Europe as an example. *Earth Planet. Sci. Lett.* **2022**, *579*, 117356. [[CrossRef](#)]
14. Bush, D.M.; Richmond, B.M.; Neal, W.J. Coastal-zone hazard maps and recommendations: Eastern Puerto Rico. *Environ. Geosci.* **2001**, *8*, 38–60. [[CrossRef](#)]
15. Quesada-Román, A.; Peralta-Reyes, M. Geomorphological Mapping Global Trends and Applications. *Geographies* **2023**, *3*, 610–621. [[CrossRef](#)]
16. Bush, D.M.; Neal, W.J.; Young, R.S.; Pilkey, O.H. Utilization of geoindicators for rapid assessment of coastal-hazard risk and mitigation. *Ocean. Coast. Manag.* **1999**, *42*, 647–670. [[CrossRef](#)]
17. Berger, A. Assessing rapid environmental change using geoindicators. *Environ. Geol.* **1997**, *32*, 36–44. [[CrossRef](#)]
18. De Pippo, T.; Donadio, C.; Pennetta, M.; Terlizzi, F.; Valente, A. Application of a method to assess coastal hazard: The cliffs of the Sorrento Peninsula and Capri (southern Italy). *Geol. Soc. Lond. Spec. Publ.* **2009**, *322*, 189–204. [[CrossRef](#)]
19. Martinez, C.; Winckler, P.; Agredano, R.; Esparza, C.; Torres, I.; Contreras, M. Coastal erosion in sandy beaches along a tectonically active coast: The Chile study case. *Prog. Phys. Geogr. Earth Environ.* **2021**, *46*, 250–271. [[CrossRef](#)]
20. Komar, P.D. Beach processes and sedimentation. *EOS Trans. Am. Geophys. Union* **1977**, *58*, 1092.
21. Van Rijn, L.C. Coastal erosion and control. *Ocean. Coast. Manag.* **2011**, *54*, 867–887. [[CrossRef](#)]
22. Alvioli, M.; De Matteo, A.; Castaldo, R.; Tizzani, P.; Reichenbach, P. Three-dimensional simulations of rockfalls in Ischia, Southern Italy, and preliminary susceptibility zonation. *Geomat. Nat. Hazards Risk* **2022**, *13*, 2712–2736. [[CrossRef](#)]
23. Caccavale, M.; Matano, F.; Sacchi, M. An integrated approach to earthquake-induced landslide hazard zoning based on probabilistic seismic scenario for Phlegrean Islands (Ischia, Procida and Vivara), Italy. *Geomorphology* **2017**, *295*, 235–259. [[CrossRef](#)]
24. de Vita, S.; Sansivero, F.; Orsi, G.; Marotta, E. Cyclical slope instability and volcanism related to volcano-tectonism in resurgent calderas: The Ischia island (Italy) case study. *Eng. Geol.* **2006**, *86*, 148–165. [[CrossRef](#)]
25. Del Prete, S.; Mele, R. Il contributo delle informazioni storiche per la valutazione della propensione al dissesto nell'Isola d'Ischia. *Rend. Soc. Geol. It Nuova Ser.* **2006**, *2*, 29–47.
26. Del Prete, S.; Mele, R. L'Influenza dei fenomeni d'instabilità di versante nel quadro morfologico della costa dell'isola d'Ischia. *Boll. Della Soc. Geol. Ital.* **1999**, *118*, 339–360.
27. Santo, A.; Di Crescenzo, G.; Del Prete, S.; Di Iorio, L. The Ischia island flash flood of November 2009 (Italy): Phenomenon analysis and flood hazard. *Phys. Chem. Earth Parts A/B/C* **2012**, *49*, 3–17. [[CrossRef](#)]
28. De Falco, M.; Forte, G.; Marino, E.; Massaro, L.; Santo, A. UAV and field survey observations on the November 26th 2022 Celario flowslide, Ischia Island (Southern Italy). *J. Maps* **2023**, *19*, 2261484. [[CrossRef](#)]
29. Selva, J.; Acocella, V.; Bisson, M.; Caliro, S.; Costa, A.; Della Seta, M.; De Martino, P.; de Vita, S.; Federico, C.; Giordano, G.; et al. Multiple natural hazards at volcanic islands: A review for the Ischia volcano (Italy). *J. Appl. Volcanol.* **2019**, *8*, 5. [[CrossRef](#)]
30. Chiesa, S.; Civetta, L.; De Lucia, M.; Orsi, G.; Poli, S. Volcanological evolution of the island of Ischia. *Rend. Acc. Sci. Fis. Mat. Napoli Spec. Issue* **1987**, 69–83.
31. Orsi, G.; De Vita, S.; Piochi, M. The volcanic island of Ischia. In Proceedings of the Volcanic Hazards and Risk in the Parthnopean Megacity, International Meeting “Cities on Volcanoes”, Rome/Naples, Italy, 28 June–4 July 1998; pp. 72–78.
32. Civetta, L.; Gallo, G.; Orsi, G. Sr- and Nd-isotope and trace-element constraints on the chemical evolution of the magmatic system of Ischia (Italy) in the last 55 ka. *J. Volcanol. Geotherm. Res.* **1991**, *46*, 213–230. [[CrossRef](#)]
33. Sbrana, A.; Marianelli, P.; Pasquini, G. Volcanology of Ischia (Italy). *J. Maps* **2018**, *14*, 494–503. [[CrossRef](#)]
34. Duperret, A.; Genter, A.; Martinez, A.; Mortimore, R. Coastal chalk cliff instability in NW France: Role of lithology, fracture pattern and rainfall. *Geol. Soc. Lond. Eng. Geol. Spec. Publ.* **2004**, *20*, 33–55. [[CrossRef](#)]
35. Hampton, M.A. Gravitational failure of sea cliffs in weakly lithified sediment. *Environ. Eng. Geosci.* **2002**, *8*, 175–191. [[CrossRef](#)]
36. Quigley, R.M.; Gelinis, P.J.; Bou, W.; Packer, R.W. Cyclic erosion–instability relationships: Lake Erie north shore bluffs. *Can. Geotech. J.* **1977**, *14*, 310–323. [[CrossRef](#)]
37. Giordano, L.; Ferrante, V.; Marsella, E.; Vicinanza, D. Coastal erosion processes modeling at Maronti Bay (Ischia Island–Southern Italy). In Proceedings of the ISOPE International Ocean and Polar Engineering Conference, San Francisco, CA, USA, 28 May–2 June 2006; p. ISOPE-I-06-123.
38. Alberico, I.; Cavuoto, G.; Di Fiore, V.; Punzo, M.; Tarallo, D.; Pelosi, N.; Ferraro, L.; Marsella, E. Historical maps and satellite images as tools for shoreline variations and territorial changes assessment: The case study of Volturmo Coastal Plain (Southern Italy). *J. Coast. Conserv.* **2018**, *22*, 919–937. [[CrossRef](#)]
39. Martínez del Pozo, J.; Anfuso, G. Spatial Approach to Medium-term Coastal Evolution in South Sicily (Italy): Implications for Coastal Erosion Management. *J. Coast. Res.* **2008**, *24*, 33–42. [[CrossRef](#)]
40. Bull, J.M.; Miller, H.; Gravley, D.M.; Costello, D.; Hikuroa, D.C.H.; Dix, J.K. Assessing debris flows using LIDAR differencing: 18 May 2005 Matata event, New Zealand. *Geomorphology* **2010**, *124*, 75–84. [[CrossRef](#)]
41. DeLong, S.B.; Prentice, C.S.; Hilley, G.E.; Ebert, Y. Multitemporal ALSM change detection, sediment delivery, and process mapping at an active earthflow. *Earth Surf. Process. Landf.* **2012**, *37*, 262–272. [[CrossRef](#)]

42. Jaboyedoff, M.; Oppikofer, T.; Abellán, A.; Derron, M.-H.; Loye, A.; Metzger, R.; Pedrazzini, A. Use of LIDAR in landslide investigations: A review. *Nat. Hazards* **2012**, *61*, 5–28. [[CrossRef](#)]
43. Hungr, O.; Leroueil, S.; Picarelli, L. The Varnes classification of landslide types, an update. *Landslides* **2014**, *11*, 167–194. [[CrossRef](#)]
44. Young, A.P.; Guza, R.T.; Flick, R.E.; O'Reilly, W.C.; Gutierrez, R. Rain, waves, and short-term evolution of composite seacliffs in southern California. *Mar. Geol.* **2009**, *267*, 1–7. [[CrossRef](#)]
45. Alberti, S.; Olsen, M.J.; Allan, J.; Leshchinsky, B. Feedback thresholds between coastal retreat and landslide activity. *Eng. Geol.* **2022**, *301*, 106620. [[CrossRef](#)]
46. Olsen, M.J.; Johnstone, E.; Driscoll, N.; Kuester, F.; Ashford, S.A. Fate and transport of seacliff failure sediment in southern California. *J. Coast. Res.* **2016**, *76*, 185–199. [[CrossRef](#)]

Disclaimer/Publisher's Note: The statements, opinions and data contained in all publications are solely those of the individual author(s) and contributor(s) and not of MDPI and/or the editor(s). MDPI and/or the editor(s) disclaim responsibility for any injury to people or property resulting from any ideas, methods, instructions or products referred to in the content.